Available online at www.sciencedirect.com
SCIENCE DIRECT®
Acta Materialia 53 (2005) 1759–1770
Acta MATERIALIA
www.actamat-journals.com

Indentation-induced phase transformations in silicon: influences of load, rate and indenter angle on the transformation behavior

Jae-il Jang [a], M.J. Lance [b], Songqing Wen [a], Ting Y. Tsui [c], G.M. Pharr [a,b,*]

[a] *Department of Materials Science and Engineering, The University of Tennessee, 434 Dougherty Engineering Building, Knoxville, TN 37996-2200, USA*
[b] *Oak Ridge National Laboratory, Metals and Ceramics Division, Oak Ridge, TN 37831, USA*
[c] *Texas Instruments Inc., 13560 N Central Expy, MS 3736, Dallas, TX 75243, USA*

Received 18 August 2004; received in revised form 13 December 2004; accepted 17 December 2004
Available online 21 January 2005

Abstract

Nanoindentation has been used widely to study pressure-induced phase transformations in Si. Here, a new aspect of the behavior is examined by making nanoindentations on (1 0 0) single crystals using a series of triangular pyramidal indenters with centerline-to-face angles varying from 35.3° to 85.0°. Effects of indenter angle, maximum load, and loading/unloading rate are systematically characterized from nanoindentation load–displacement data in conjunction with micro-Raman imaging spectroscopy of the residual hardness impressions. Results are discussed in terms of prevailing ideas and models for indentation-induced phase transformations in silicon.

Keywords: Nanoindentation; Phase transformations; Silicon; Raman spectroscopy

1. Introduction

During indentation, the material in the sample directly beneath the rigid diamond indenter experiences very intense localized stresses and strains. In a small number of semiconductors and ceramic materials, these high stresses can cause plastic deformation not only by dislocation activity, but also by pressure-induced phase transformations to denser crystalline and amorphous forms [1–4]. In addition to being a scientific curiosity, the transformation to the high pressure phase has technological importance in the way it facilitates precision machining of these materials by enhancing ductile mechanisms of cutting [5–7].

It is well known through diamond anvil cell (DAC) experiments and theoretical studies [8–11] that silicon transforms from the diamond cubic structure (dc) denoted Si-I to the metallic β-tin structure (Si-II) at a hydrostatic pressure in the range 11–13 GPa. On release of the pressure, the material first reverts to Si-XII (r8) and then to Si-III (bc8) [10,12,13]. In the 1970s, Gridneva et al. [14] and then Gerk and Tabor [15] suggested that the transformation from Si-I to Si-II also occurs during indentation, and that it may play an important role in determining the hardness of the material. A decade later, Clarke et al. [16] reported that there is a region of amorphous material near the center of unloaded Vickers and Knoop indentations, illustrating another curious aspect of the transformation.

Research in the field accelerated in the late 1980s with the development of load and depth sensing indentation techniques (nanoindentation), which made it possible to investigate the mechanical response during the entire sequence of loading and unloading. Since the work of Pharr et al. [17], who reported unique features in unloading curve shape of Si during nanoindentation,

* Corresponding author. Tel.: +1 865 974 8202; fax: +1 865 974 4115.
E-mail address: pharr@utk.edu (G.M. Pharr).

1359-6454/$30.00
doi:10.1016/j.actamat.2004.12.025

numerous nanoindentation studies [18–23] have been performed to examine the phase transformations in Si. In the late 1990s, Kailer et al. [24] observed the metastable Si-XII/Si-III crystalline phases and an amorphous phase after indentation using micro-Raman techniques. They argued that the high-pressure Si-II phase transforms to the amorphous state during rapid unloading, whereas the crystalline phases form upon a slow load release. Over the past 5 years, a large number of studies have been conducted to further characterize the behavior through various experimental techniques, including plan-view [25–30] and cross-sectional [31–37] transmission electron microscopy (TEM), electrical resistance measurements [38–40], and micro-Raman spectroscopy [29,30,33,41–44].

As reviewed by Domnich and Gogotsi [45], it is apparent that the transformation mechanisms are dependent on the indentation testing conditions, e.g., peak load and loading/unloading rate. This implies that the transformation could potentially be controlled in a manner which could prove useful in improving the precision machining of Si. Nevertheless, how the major controllable parameters and their interactions affect the transformation process is not yet fully understood.

With this in mind, we systematically examine here the role of several indentation parameters on the physics of the transformation process by carefully analyzing micro-Raman spectra and nanoindentation load–displacement curves. In addition to the peak load and loading/unloading rate often examined in the past, a new variable is introduced: the sharpness of the triangular pyramidal indenter as characterized by its centerline-to-face angle, Ψ. In general, sharper indenters induce larger stresses and strains in the material due to the larger volume of material that is displaced. Six different indenters were employed in the study with angles varying in the range 35.3°–85.0°. As might be expected, a wide variety of transformation behaviors were observed depending on the sharpness of the indenter. The new observations provide important new clues about the transformation processes and the way they might affect machining performance.

2. Experimental procedure

Nanoindentations were made on standard wafers of (1 0 0) Si using a Nanoindenter-XP (MTS System Corp., Oak Ridge, TN). Six different triangular pyramidal indenters were employed having centerline-to-face angles, Ψ, of 35.3° (cube-corner), 45.0°, 55.0°, 65.3° (Berkovich), 75.0°, and 85.0°. Loads were varied in the range from 1 to 100 mN and loading/unloading rates from 0.05 to 5 mN/s. Values of hardness (H) and Young's modulus (E) obtained from the load–displacement data for the Berkovich indentations using the Oliver–Pharr method [46] were H = 11.5 to 12.5 GPa and E = 160 to 165 GPa.

After testing, micro-Raman analyses were conducted using a Dilor XY800 Microprobe (JY Inc., Edison, NJ) to identify any crystalline and amorphous phases that were present after unloading. The scattered light from an Innova 308c Ar^+ laser (Coherent Inc., Santa Clara, CA) operating at 5145 Å was dispersed with a diffraction grating and then detected with a charge-coupled device (CCD). Using an average laser spot size of approximately 1 μm, Raman spectral maps of the indents were acquired automatically using mapping software. For comparison, all the hardness impressions were also imaged using a Leo 1525 field-emission scanning electron microscopy (Carl Zeiss SMT Inc, Thornwood, NY) to identify important topographical features. One indentation was cross-sectioned by dual-beam focused ion beam (FIB) milling for TEM examination.

3. Influences of indenter angle and indentation load

Ever since it was reported [17] that there is a very reproducible discontinuity in unloading curves at high peak loads (>30 mN) and hysteresis loops during cyclic nanoindentation at low peak loads (<20 mN), these unique material behaviors that occur during the nanoindentation of Si with a Berkovich indenter (Ψ = 65.3°) have received a great deal of attention. Recently, Gogotsi and co-workers [42–45] suggested based on post-indentation micro-Raman studies that there is a good correlation between the unloading curve shape and the final structure of the transformed material. They proposed that the unloading discontinuity, often called the 'pop-out', corresponds to the formation of metastable Si-XII/Si-III crystalline phases, while the hysteresis, called the 'elbow' for one-cycle of loading and unloading, is associated with the formation of amorphous Si (a-Si). They also reported that higher maximum loads (50 mN) lead to pop-out while lower loads (30 mN) produce the elbow [42–45].

The studies conducted here show that the pop-out and elbow behavior also depend on the indenter angle. Typical examples of the pop-out and elbow are shown in Fig. 1. Since the elbow is difficult to clearly identify during one-cycle of loading/unloading (in comparison to cyclic indentations), the presence or absence of pop-out rather than elbow will be the main focus in this work.

Fig. 2 shows some representative examples of load–displacement (P–h) curves obtained at high and low loads (P_{max} = 80 and 13 mN), and Table 1 lists a summary of the unloading curve characteristics obtained from nanoindentations at a fixed loading/unloading rate (dP/dt) of 5 mN/s. The figure and table show that the

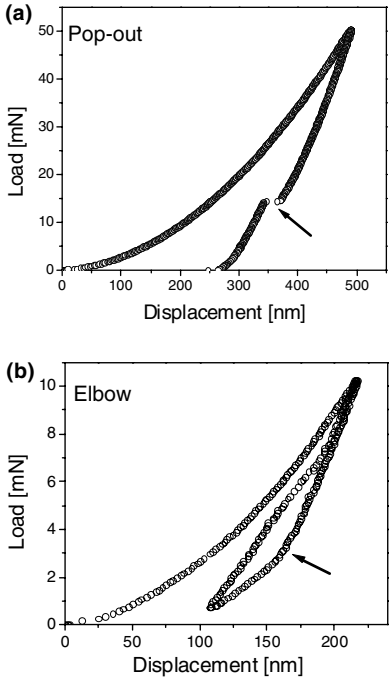

Fig. 1. Typical examples of pop-out and elbow observed in nanoindentation P–h curves: (a) pop-out and (b) elbow.

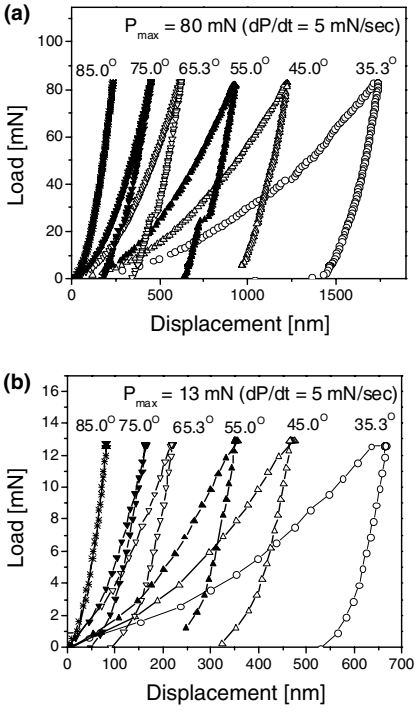

Fig. 2. Variations in load–displacement curves with changes in centerline-to-face angle, Ψ, and maximum load: P_{max} = (a) 80 mN and (b) 13 mN. Results are from nanoindentations at a fixed loading/unloading rate dP/dt = 5 mN/s.

pop-out and elbow behavior commonly reported for the Berkovich indenter are also clearly observed for the 55.0° indenter, i.e., at relatively high loads pop-out is observed, with the elbow behavior appearing at low loads. However, for 35.3° and 45.0° indenters, there is no pop-out at any load, a somewhat surprising observation since these sharper indenters are expected to displace more volume than the 55.0° and 65.3° indenters and therefore produce a greater amount of transformed material. The very blunt 85.0° indenter exhibits purely elastic contact, as evidenced by the fact that the loading and unloading curves are identical, and the 75.0° indenter exhibits a small elbow at high loads (sometimes, followed by a small pop-out).

To examine the elbow behavior at low loads in more detail, cyclic indentations were made as shown in Fig. 3.

In a manner similar to the previous observations by Pharr et al. [17], indentations made with the 65.3° (Berkovich), 55.0° and 45.0° indenters exhibit a large hysteresis loop with no signs of degeneration through several cycles of deformation, while a very small hysteresis is observed for the 75.0° indenter. In contrast, the loading/unloading curves for the cube-corner indenter show a small hysteresis in the first cycle (see Fig. 3(b) and (c)), but the looping degenerates and disappears in higher cycles. Eventually, the loading and unloading curves become virtually indistinguishable characteristic of perfectly reversible elastic deformation. We will return to this issue later.

Table 1
Summary of unloading curve characteristics as a function of peak indentation load (P_{max}) and indenter angle (Ψ)

	Indenter angle, Ψ (°)					
	35.3	45.0	55.0	65.3	75.0	85.0
P_{max} (mN)						
100	No	No	P	P	E (P)	F
80	No	No	P	P	E (P)	F
50	No	No	P	P (E)	E	F
30	No	No	P (E)	E (P)	E	F
20	No	E	E (P)	E (P)	E	F
10	No	E	E	E	E	F

All nanoindentations were made at a loading/unloading rate of 5 mN/s.
Notations in the table are; No, no pop-out/elbow; P, pop-out; E, elbow; P (E), mainly pop-out (mixed with elbow); E (P), mainly elbow (mixed with pop-out) and F, fully elastic behavior.

Typical micro-Raman analysis results are presented in Fig. 4. These Raman spectra were obtained from the center of each indentation using a laser spot size of about 1 μm. The sharp peak at 521 cm^{-1} represents pristine Si-I, but the broader peaks around 150, 300, and 470 cm^{-1} and the narrow bands at 165, 350, 382, 395, and 430 cm^{-1} were identified as a-Si and Si-XII/Si-III, respectively, in agreement with previous studies [24,41–45]. Except for the 75.0° indenter, which exhibits mostly Si-I with a little a-Si mixed in, the Si-XII/Si-III phases are formed at high loads for all the indenters. With decreasing load, the peaks of the crystalline phases diminish and the amorphous peaks become stronger. Curiously, for the sharpest indenter (35.3°), the crystalline peaks are relatively weak compared with other indenters. If the results from the 35.3° indenter are analyzed separately, as shown in Fig. 5, a clear dependence of the structure on the peak load is apparent. The intensity of the crystalline peaks decreases as the peak load is decreased, and at very low loads (10 and 20 mN), only an a-Si peak at 470–480 cm^{-1} or an a-Si peak combined with a nanocrystal cubic diamond Si (nano-Si) peak at 500–510 cm^{-1} [41,45,47] is observed. Although it is hard to accurately evaluate the relative amounts of nano-Si and a-Si because their peaks are broad and partially overlap with themselves and the Si-I peak, the presence of the nano-Si (which may crystallize from the a-Si, either on its own at room temperature or as activated by Raman laser heating [41]) is clearly observed in Fig. 5.

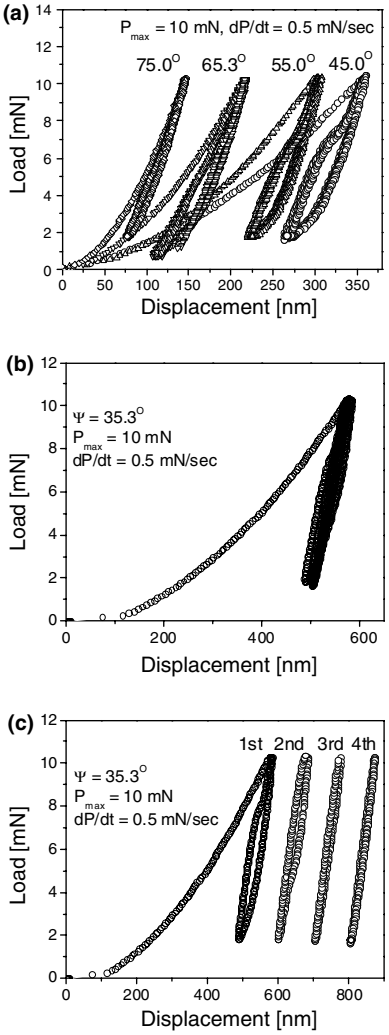

Fig. 3. Load–displacement curves obtained from cyclic nanoindentations made at P_{max} = 10 mN and a loading/unloading rate of 0.5 mN/s: (a) variations in the curve characteristics for indenter angles varying from 45.0° to 75.0°; (b) a curve for the cube-corner indenter (Ψ = 35.3°); (c) result from (b) separated for clarity.

Comparison of Table 1 and Fig. 4 confirms that for the 55.0°, 65.3°, and 75.0° indenters there is a strong relationship between the unloading curve shape and the structure of transformed material in a manner, consistent with the suggestions of Gogotsi and colleagues [42–45]; specifically, pop-out corresponds to the formation of the crystalline phases and the elbow to the formation of a-Si. Curiously, however, the indentations made with the 35.3° and 45.0° indenters do not show pop-out.

The micro-Raman spectra show clearly for each indenter that the crystal structure of the transformed material depends on the peak load. An important question arising from these results is why a geometrically self-similar pyramidal indenter should yield different transformed material given that the stress distribution under the indenter should also be self-similar. One possible answer is that given by Domnich and Gogotsi who suggested in their review article [45] that "a-Si rather than Si-XII forms during unloading of indentations made at very low loads (<10 mN) because the transforming volume in this case is probably too small to allow the reconstructive (Si-II)-to-(Si-XII) transformation." Since reconstructive transformations generally require nucleation and growth, the density and distribution of nucleation sites is an important controlling factor. Thus, if the indentation is made at high loads, the transformed volume of the Si-II phase during loading may be large enough to have sufficient nucleation sites for the Si-XII/Si-III phases, whereas for small transformed volumes at low loads, the probability of nucleation event is reduced.

In this regard, it is constructive to consider how the transformed volume depends on the indenter angle. Although precise quantification cannot be achieved due to the complex nature of deformation processes involved as well as the unknown nature of the elastic and plastic properties of the transformed material, some insight into important phenomena can be gained by considering fully elastic and elastic-perfectly-plastic models for indentation by a rigid cone. In order to relate conical indentation results to those obtained by triangular pyramidal indenters, it is useful to make the normal assumption that similar behavior is obtained when the angle of

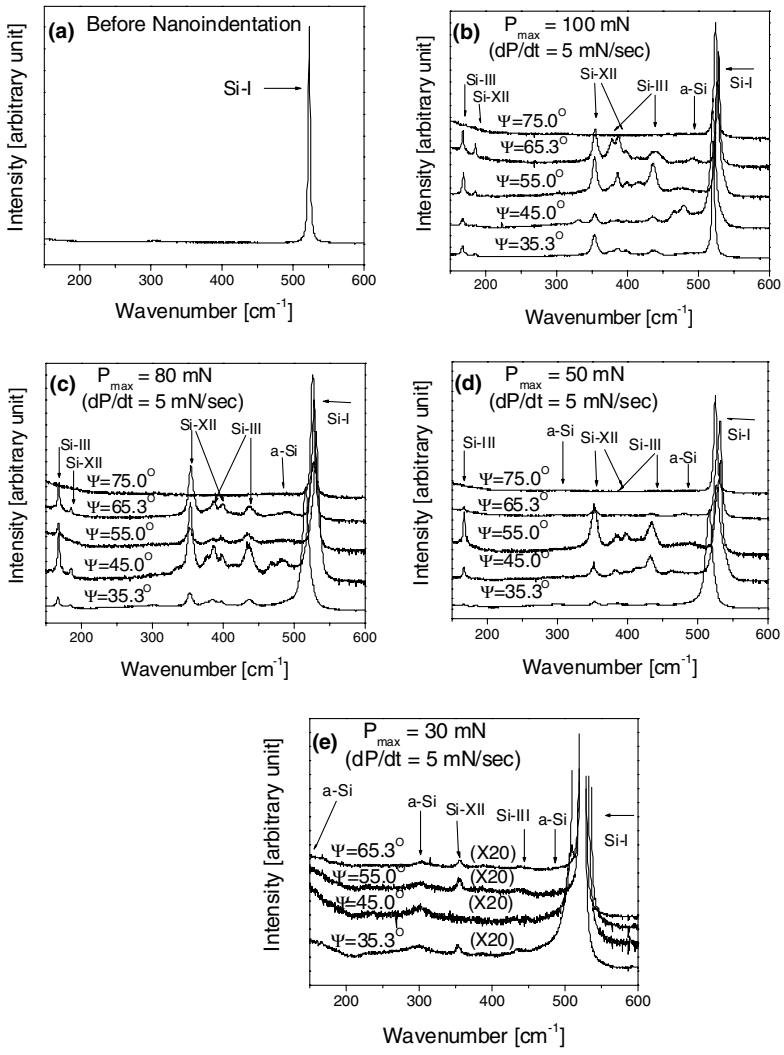

Fig. 4. Raman spectra from nanoindentations made with different indenters at various maximum loads: (a) original Si before nanoindentation; P_{max} = (b) 100 mN; (c) 80 mN; (d) 50 mN; and (e) 30 mN (intensity resolution increased by 20×).

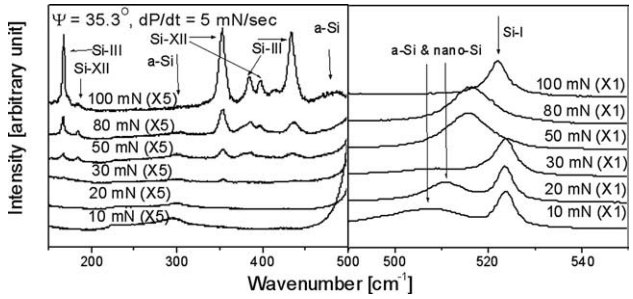

Fig. 5. Micro-Raman spectra from nanoindentations made with a cube-corner indenter at various maximum loads.

the cone gives the same area-to-depth relation as the pyramid. For example, for the Berkovich indenter, the equivalent cone angle is 70.3°, and for the cube-corner 42.3°.

Sneddon [48,49] has provided a comprehensive treatment of elastic contact by a rigid cone with half included angle, Ψ. Of particular interest here is the distribution of pressure under the indenter given by

$$p(r) = \frac{E}{2(1-\nu^2)} \frac{\cosh^{-1}(a/r)}{\tan \Psi}, \quad 0 \leqslant r \leqslant a, \tag{1}$$

where E is Young's modulus, ν is Poisson's ratio, a is the contact radius, and r is the radial coordinate in the surface. Although the real pressure distribution will be truncated in the center due to the transformation, this equation suggests two important points: (1) the pressure increases with decreasing indenter angle and (2) higher pressures are sustained to larger fractions of the contact radius for indenters with smaller angles. Since the contact radius of Si does not change significantly with indenter angle (this is borne out by experimental observations that the hardness of Si is essentially independent of indenter angle [50]), these effects help to explain why extrusion occurs only for the sharper indenters, as will be discussed in the next section.

Important insights may also be gained using Johnson's expanding cavity model for elastic–plastic indentation with a cone [51]. According to the model, the relationship between the plastic zone radius, b, and indenter angle is:

$$\frac{b}{a} = \left\{ \frac{1}{6(1-\nu)} \left[\frac{E}{\sigma_{YS}} \tan(90^\circ - \Psi) + 4(1-2\nu) \right] \right\}^{1/3}, \tag{2}$$

where σ_{YS} is the yield stress. If we assume that the transformed zone of the high pressure Si-II behaves like the plastic zone and that the contact radius, a, of Si is approximately independent of indenter angle [50], the form of Eq. (2) suggests that the volume of the transformed zone will increase with increasing sharpness (i.e., decreasing indenter angle). Thus, if the transformed volume is important in nucleation, sharp indenters should show a greater tendency to form the Si-XII/Si-III phases than blunt indenters. This expectation is in good agreement with the micro-Raman data in Fig. 4. Close inspection shows that the minimum load needed for transformation to the crystalline phases increases with decreasing sharpness (increasing angle). Specifically, this load is around 30 mN for 35.3–55.0° indenters, around 50 mN for the 65.3° indenter, and is expected to be more than 100 mN for the 75.0° indenter. Thus, decreasing the indenter angle and increasing the peak load, both of which increase the volume of Si-II, are expected to promote the reversion to the crystalline Si-XII/Si-III forms. Since the transformed volumes are very small, it is not surprising that a single nucleation event can dominate the process and that the nucleation event can therefore be experimentally observed.

An important inference from these observations is that one may be able to control the nature of the final transformation products by changing the peak load or the indenter angle. To explore this hypothesis, additional indentation tests were performed at a peak load of 500 mN with the 75.0° indenter, which showed just a little a-Si as transformed material at 100 mN. Extrapolation of the observations in Fig. 4 suggests that the Si-XII/Si-III phases should appear at this higher load. The micro-Raman data obtained are shown in Fig. 6(a). Unlike the results from 80 and 100 mN (also shown in the figure), the spectra for the indentation at 500 mN indicate the clear presence of Si-XII/Si-III, as well as some amorphous material, and the Si-I peak is almost entirely absent. Also, a clear pop-out corresponding to the transformation to the Si-XII/Si-III phases is observed in the P–h curves, as shown in Fig. 6(b).

Collectively, these results suggest that a sufficient transformed volume of Si-II is needed to form the Si-XII/Si-III crystalline phases during unloading, and that increases in sharpness and load individually enhance the formation because the transformed volume scales with

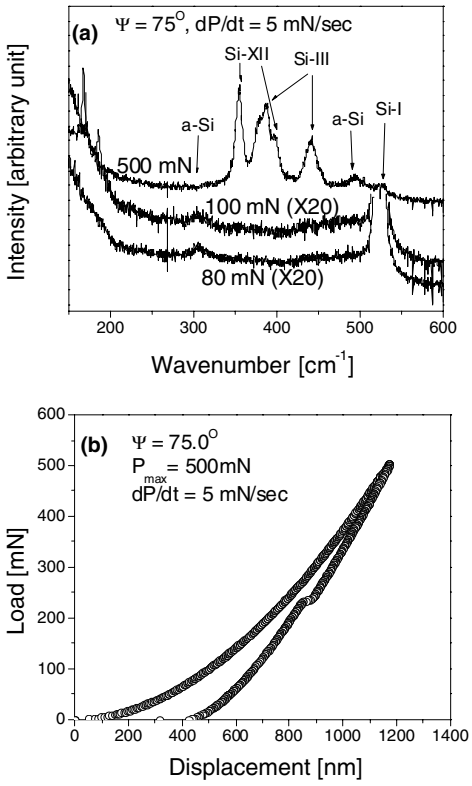

Fig. 6. Data for high load indentations made with the 75° indenter: (a) micro-Raman spectra; and (b) the P–h behavior at P_{max} = 500 mN.

these parameters. As mentioned previously, since all these suggestions are based on qualitative analysis of the observed phenomena, further efforts to develop a precise way to quantify critical conditions for the transformation under different indenters are desirable for better understanding of the phenomena. Recently, Galanov et al. [52] developed a contact-mechanics model based on expanding cavity concept, for the phase transformation under a Berkovich indenter. Although a good first attempt, the model ignores several important factors such as cracking and the actual shape of transformed zone that may influence the transformation in a significant way. A more accurate description of the phenomena may conceivably be achieved by three-dimensional finite element analysis if the volumetric change due to the different densities of the Si phases and the elastic–plastic properties of the transformed Si are incorporated.

4. The importance of extrusion

An important unresolved question is why the pop-out during unloading does not occur for high-load indentations with the 35.3° and 45.0° indenters, even though the Si-XII/Si-III phases are clearly observed in the micro-Raman spectra. A clue is provided in

Fig. 7, which shows a series of scanning electron microscopy (SEM) images of nanoindentations at a peak load of 80 mN with different indenters. For the 85.0° indenter, contact is purely elastic, so no remnant indentation is produced and no micrograph is shown. The important feature in the micrographs is the thin, extruded material at the contact periphery seen clearly for the 35.3° and 45.0° indenters, but not the others. Since Pharr et al. [18] first observed this phenomenon in studies conducted with a cube-corner indenter ($\Psi = 35.3°$), the metal-like plastic flow behavior of the extruded material has been taken as evidence of transformation to the ductile metallic Si-II phase at high pressures [5,45]. Fig. 7 shows that there is an abundance of extruded material for the cube-corner indenter ($\Psi = 35.3°$), a lesser amount for the 45.0° indenter, and no extrusion at all for $\Psi = 55.0°$, 65.3°, and 75.0° indenters.

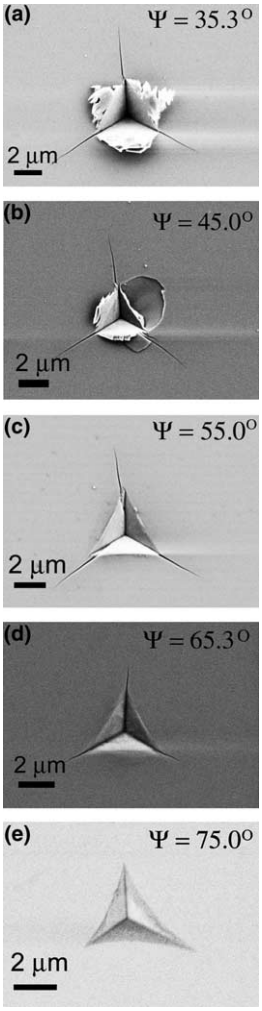

Fig. 7. SEM micrographs of nanoindentations made with indenters of various angle at $P_{max} = 80$ mN and $dP/dt = 5$ mN/s; (a) 35.3° (cube-corner indenter); (b) 45.0°; (c) 55.0°; (d) 65.3° (Berkovich indenter); and (e) 75.0°. Note that the magnification of each image is not the same.

Fig. 8 shows some additional features of the extrusion behavior. In Fig. 8(a), the geometry of the extruded material for the cube-corner indenter is seen in cross-section in a TEM image. It is clear that the extrusions extend from a thin layer of highly plastic material that is sandwiched between the diamond tip and the relatively hard surrounding Si-I. For cube-corner indentations, the extrusion is extensive and observed both at high and low loads (Figs. 7(a) and 8(b)–(d)). In contrast, the amount of extrusion for the 45.0° indenter is smaller (Figs. 7(b) and 8(e)), and extrusion is not evident at the lowest load of 10 mN (Fig. 8(f)).

Comparison of the micrographs in Fig. 7 with the P–h curves in Fig. 2(a) shows that the presence of the extruded material correlates with the absence of pop-out at high loads for the 35.3° and 45.0° indenters. The model we propose to explain this behavior is based on the dependence of the pressure distribution under the indenter on the indenter angle. Fig. 9 shows schematically the relationship between the pressure distribution for elastic contact and the possible distribution of the transformed zone of the high pressure Si-II phase. Note that it is possible to assume that contact radius is constant for all indenters based on the observation that the hardness of silicon is essentially independent of indenter angle [50]. As elaborated in the previous section, sharper indenters produce greater pressures, p, and the greater pressures extend to greater fractions of the contact radius (Fig. 9(a)) [48,49]. However, the real pressure distributions are limited by the phase transformation from Si-I to Si-II ($P_{I\rightarrow II}$), well known to be 11–13 GPa. When the phase transformation occurs, the pressures under the indenter are truncated to lower values, which to a first approximation are limited by the transformation pressure as indicated by the dashed horizontal line in the figure. The salient point is that the transformation zone for sharp indenters is then expected to extend to a much greater fraction of the contact radius than for blunt indenters, as shown in Fig. 9(b). Thus, the likelihood that the metallic phase can escape from under the contact to the free surface at the contact edge is greater for sharper indenters. For blunt indenters, the transformed zone is small, and flow of the metallic Si-II phase is inhibited by the surrounding untransformed material. Based on the observations in Fig. 7, the critical angle for escape of the metallic material to the free surface appears to be in the 45.0–55.0° range for a pyramidal indenter.

Once extrusion occurs during indentation, the hydrostatic pressure in the extruded material is immediately released, and it should therefore transform to a low-pressure phase. Since the pressure release occurs quickly, there is insufficient time for the phase transformation from Si-II to the Si-XII/Si-III crystalline phases (Section 5). Thus, the extruded Si-II transforms directly into a-Si (or possibly nano-Si). While the extrusion is occurring, some the

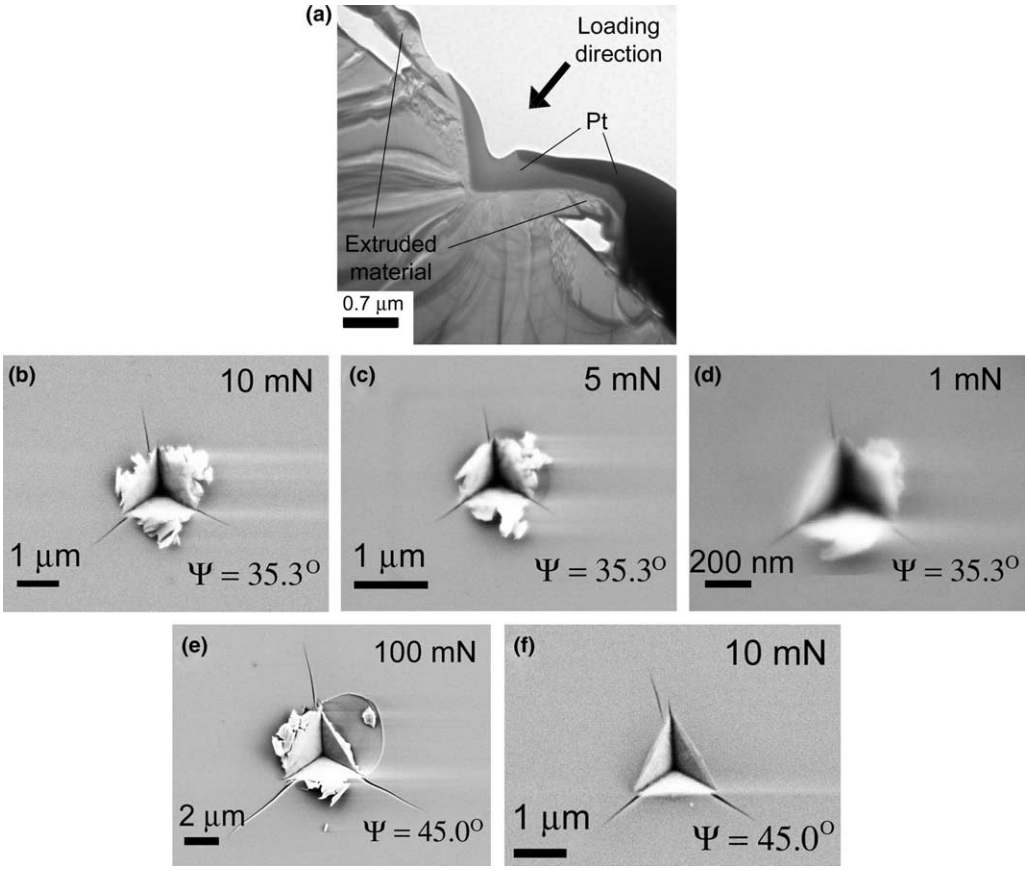

Fig. 8. Examples of extruded material observed with the 35.3° and 45° indenters: (a) cross-sectional TEM image obtained from a region close to the corner of hardness impression (P_{max} = 80 mN); (b–d) SEM images of low load indentations for the cube-corner indenter (35.3°); and (e–f) SEM images of high and low load indentations for the 45.0° indenter.

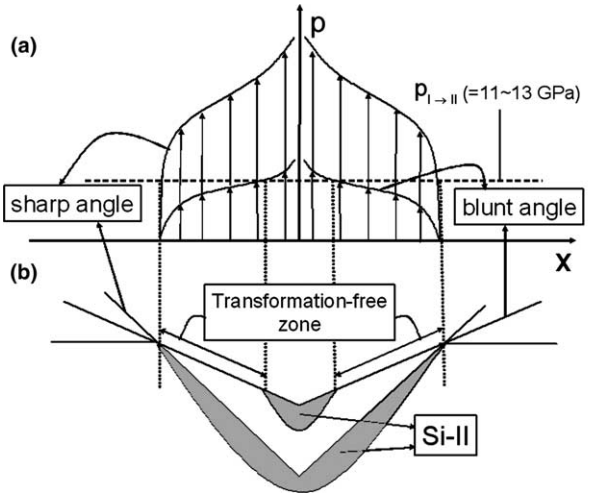

Fig. 9. Schematic illustration of difference in extrusion behavior for a sharp indenter (such as the cube corner) and relatively blunt indenter (Berkovich): (a) pressure distribution for elastic contact, and (b) distribution of transformed Si-II in corresponding to pressure distribution in (a).

Si-II near the center of the indent cannot reach the surface and remains trapped between the indenter tip and the hard Si-I material. During unloading, this residual Si-II phase transforms to Si-XII/Si-III phases or a-Si at relatively high and low loads, respectively.

To further explore this proposed mechanism, micro-Raman mapping techniques were applied to the cube-corner indentations with extruded material (see Fig. 10(a)). By making maps with either the a-Si/nano-Si peak or Si-XII/Si-III crystalline peak in the Raman spectra (Fig. 10(b)), the spatial locations of each of these materials were identified (Fig. 10(c) and (d)). Comparing these maps with the SEM micrographs verifies that the extruded material is a-Si (or nano-Si) and that small amounts of the Si-XII/Si-III phases are formed near the impression center.

Finally, the absence of unloading pop-out for the 35.3° and 45.0° indentations can also be explained by the extrusion behavior. Since a large amount of Si-II is extruded in the cube-corner indentation, the reverse transformation from Si-II is very limited and thus there is no pop-out. Similarly, for the 45.0° indenter, which shows extruded material only at high loads (Figs. 7(b) and 8(e)), there is no pop-out in the high load regime. The nature of the hysteresis loops at low loads shown in Fig. 3 can also be explained by the hypothesis. For the 75.0°, 65.3°, and 55.0° indenters (Fig. 3(a)), the non-degenerative hysteresis results from the transform-

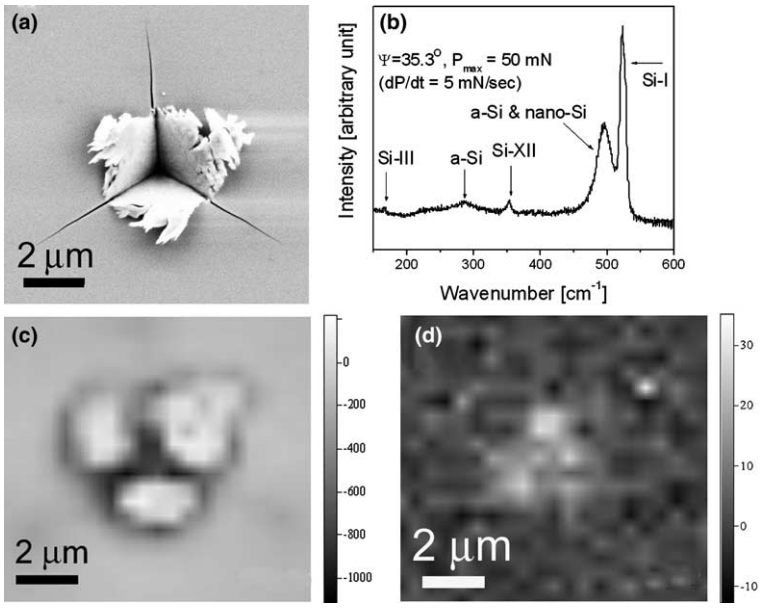

Fig. 10. Cube-corner indentation made at P_{max} = 50 mN and dP/dt = 5 mN/s: (a) SEM image; (b) typical micro-Raman spectrum; (c) micro-Raman map identifying amorphous and nanocrystalline Si phases; (d) micro-Raman map identifying metastable crystalline phases (Si-III and Si-XII). In (c–d), the lighter regions correspond to the phase used to create the map.

ing material being trapped under the indenter and therefore reversibly transforming back and forth with corresponding volume changes. The relatively small size of the hysteresis for 75.0° indenter is due to the limited volume of transforming material. Since for the 45.0° indenter the extruded material disappears at low loads (as shown in Fig. 8(f)), a large hysteresis loop is also observed for the 45.0° indenter (see Fig. 3(a)). On the other hand, for the cube-corner indenter (Ψ = 35.3°; Fig. 3(b) and (c)), the transforming material extrudes out even at low loads (Fig. 8(b)–(d)) and the indenter displacement associated with the reverse transformation is not significantly recovered.

5. Rate effects

It is well-known that in Berkovich and spherical indentation, the loading/unloading rate also affects the transformation behavior. Even at low loads where only the elbow is observed at typical indentation rates (see Fig. 3), very slow unloading can yield pop-out behavior [24,33,40]. To evaluate rate effects for the indenters examined in this study, tests were conducted to peak loads of nominally 10 mN at dP/dt = 0.05 and 0.5 mN/s. The load–displacement curves are presented in Fig. 11.

For extremely blunt indenters (Ψ = 85.0° and 75.0°), no obvious change in the unloading curve is observed with decreasing rate. This is not surprising for the 85.0° indenter because it induces purely elastic behavior. For the 75.0° indenter, the transformed volume of Si-II is presumably so small that there are insufficient nucleation sites to form the Si-XII/Si-III crystalline phases on unloading. The behavior of the 65.3°, 55.0°, and 45.0° indenters, which is qualitatively similar, is characterized by a change in unloading curve shape from elbow to pop-out with decreasing unloading rate. This

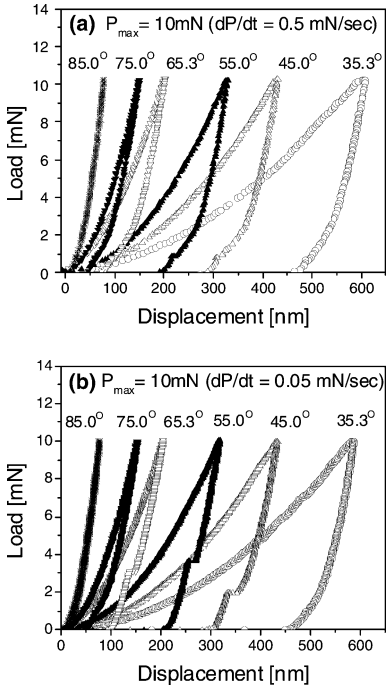

Fig. 11. Dependence of P–h curves on the loading/unloading rate for indentations made at P_{max} = 10 mN: dP/dt = (a) 0.5 mN/s; and (b) 0.05 mN/s. Results for 5 mN/s are shown in Fig. 2(b).

is consistent with the hypothesis that the pop-out is kinetically limited by the nucleation of Si-XII/Si-III from Si-II; that is, slower unloading rates provide more time for the nucleation event to occur. Note that the 45.0° indenter, which did not induce extruded material at P_{max} = 10 mN (see Fig. 8(f)), indicates clear pop-out behavior at the slowest rate of 0.05 mN/s. For the 35.3° indenter, there is no change in the unloading curve behavior due to the extensive extrusion of transformed material (see Fig. 8(b)).

Several attempts were made to characterize the structures formed for the indentations in Fig. 11 by micro-Raman analysis, but due to their small size, most could not be imaged. The technique was successful only for the cube-corner indentations for which the large cracks and extruded material helped to identify the locations of the indentations. Micro-Raman spectra obtained from the cube-corner indentations are shown in Fig. 12. The data exhibit a trend similar to varying the indenter angle: the peak intensity of the a-Si and nano-Si phases decreases with decreasing unloading rate, and at very low rates (such as 0.05 mN/s) the crystalline Si-XII phase peak emerges. This demonstrates that for the 35.3° indenter, the small amount of Si-II phase remaining in the hardness impression after extrusion can indeed transform to the crystalline Si-XII form if the unloading rate is slow enough.

This rate dependency of the transformation can be explained by the nature of the nucleation and growth process [16,24,40]. The first attempt to explain the formation of the amorphous phase was made by Clarke et al. [16], who identified amorphous Si in Vickers and Knoop indentations and proposed two possible mechanisms: (1) a structural kinetic argument, i.e., that at a rapid unloading rates, the Si-II phase cannot transform to another crystalline phase because of kinetic barriers to nucleation and growth and (2) direct amorphization, in which Si-I transforms directly to a high pressure amorphous phase when the local pressure exceeds the metastable extension of the liquidus curve in the P–T diagram, and the amorphous phase persists on unloading because of insufficient thermal energy to allow rearrangement back to Si-I. The former explanation is generally thought to be more plausible because direct conversion should require a pressure of approximately 24 GPa [16], which is considerably higher than the hardness of Si (about 12 GPa).

Bradby et al. [40] recently proposed that during unloading of Si-II, there may be a kinetic barrier to nucleation of the Si-XII/Si-III phases but no barrier to amorphization. The results in this study are consistent with this hypothesis. The mechanism we envisage involves the formation of Si-II during loading which converts either to amorphous silicon or Si-XII/Si-III depending on the volume of transformed material and the unloading rate. If the rate is fast, there is insufficient time for the nucleation of the crystalline phases and a-Si is formed. For slow unloading, the crystalline phases nucleate and grow. In order to explain the pop-out, it must be assumed that the transformation kinetics are rate limited by nucleation; that is, after one nucleus forms, its growth is so rapid so that the reverse transformation is completed over a very short period of time. For sharper indenters, the transformation behavior is complicated by the extrusion of the Si-II phase. The extrusions themselves are amorphous due to the rapidity with which the material decompresses. The material

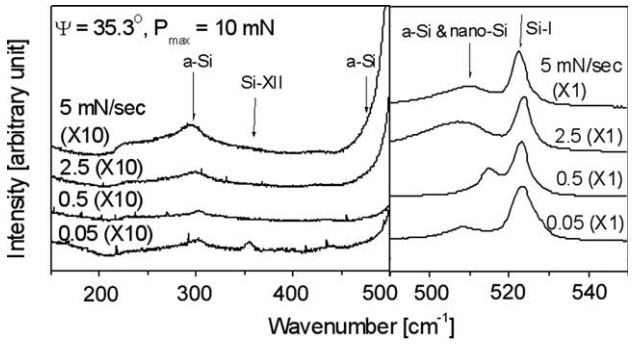

Fig. 12. Dependence of micro-Raman spectra on the loading/unloading rate for nanoindentations made with cube-corner indenter at P_{max} = 10 mN.

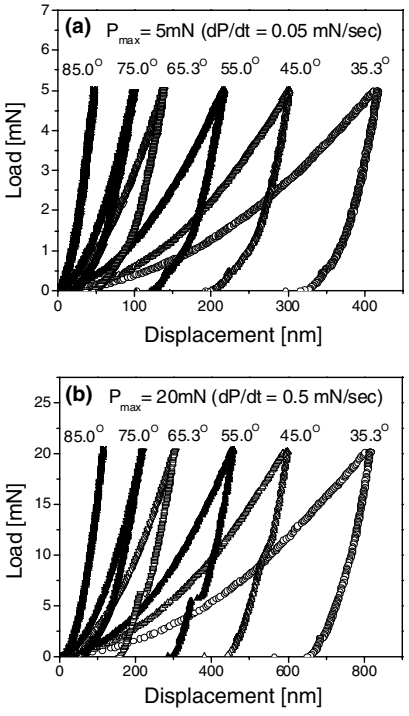

Fig. 13. Additional P–h curves obtained from nanoindentations at low loads; P_{max} = (a) 5 mN (dP/dt = 0.05 mN/s); and (b) 20 mN (dP/dt = 0.5 mN/s).

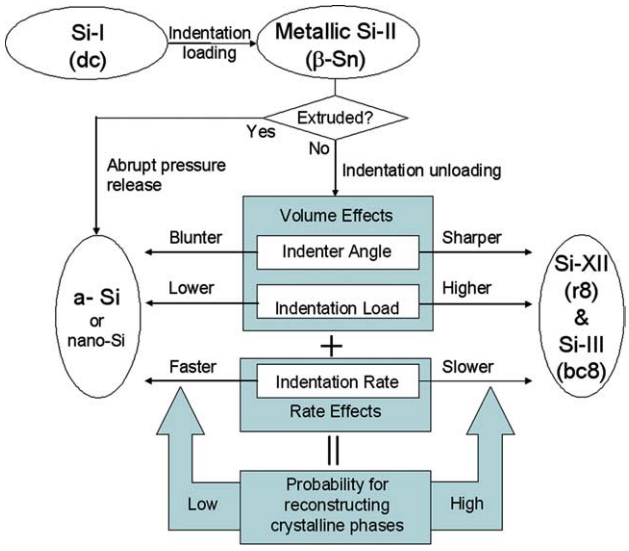

Fig. 14. Schematic illustration of phase transformation processes and influences of indentation testing parameters on them.

remaining under the indenter then transforms to amorphous or crystalline depending on the unloading rate.

Another interesting tendency found in this study is that the rate of transformation to Si-XII/Si-III may vary with peak loads for all the indenters. Fig. 13 shows some additional P–h curves obtained at low peak loads of 5 and 20 mN. Unlike the 10 mN indentation results in Fig. 11(b), the 5 mN indentations in Fig. 13(a) do not show pop-out at 0.05 mN/s, which means that at 5 mN a rate slower than 0.05 mN/s is needed for transformation to the crystalline phases. On the other hand, the indentations to $P_{max} = 20$ mN show clear pop-out at 0.5 mN/s (Fig. 13(b)), at which pop-out is not observed in the 10 mN indentations (see Fig. 11(a)). Note that, at higher loads such as 50 and 80 mN, the crystalline phases are normally observed in indentations at the relatively fast rate of 5 mN/s. This implies that rate effects are coupled with the volume effects, i.e., the large volume of Si-II may be helpful in reducing the time required for transformation from Si-II to the Si-XII/Si-III phases. Based on these ideas, complete amorphization in Berkovich nanoindentations at high loads ($P_{max} \geqslant 80$ mN) may be possible if the indentation is unloaded at very fast rates (as in impact events). Additionally, this is consistent with the fact that the 75.0° indenter, which produces a small volume of Si-II, does not show pop-out even at very slow rates, as shown in Fig. 11(b).

6. Conclusions

Using six three-sided pyramidal indenters having centerline-to-axis angles from 35.3° to 85.0°, the influence of various nanoindentation testing parameters on indentation-induced phase transformations in Si has been systematically examined. The possible transformation processes predicted from examination of micro-Raman spectra and indentation P–h curves are schematically summarized in Fig. 14. During the indentation loading sequence, Si-I transforms to the metallic Si-II phase under high pressure. If the indenter angle is very sharp (e.g., cube-corner indenter), material is extruded out of the hardness impression and immediately transformed into a-Si or nano-Si. Upon unloading, the Si-II phase which was not extruded and remains under the indenter re-transforms to the a-Si phase or the metastable crystalline Si-XII/Si-III phases. Which transformed phases form is determined by the indenter angle, indentation peak load, and indentation rate in the manner described in the figure. Since each of these parameters have counterparts that can be controlled in single point diamond turning operations, the observations could prove useful in improving our ability to perform precision machining operations in silicon and other materials exhibiting pressure-induced phase transformations.

Acknowledgments

This research was sponsored by the National Science Foundation under Grant No. DMR-0203552, and by the Division of Materials Sciences and Engineering (SHaRE User Center), U.S. Department of Energy, under Contract DE-AC05-00OR22725 with UT-Battelle, LLC.

References

[1] Domnich V, Gogotsi Y. In: Halwa HS, editor. Handbook of surfaces and interfaces of materials, vol. 2. New York: Academic Press; 2001. p. 195.
[2] Gilman JJ. J Mater Res 1992;7:535.
[3] Schmücker M, Schneider H, Kriven WM. J Am Ceram Soc 2003;86:1821.
[4] Ge D, Domnich V, Juliano T, Stach EA, Gogotsi Y. Acta Mater 2004;52:3921.
[5] Tanikella BV, Somasekhar AH, Sowers AT, Nemanich RJ, Scattergood RO. Appl Phys Lett 1996;69:2870.
[6] Gogotsi YG, Kailer A, Nickel KG. Nature 1999;401:663.
[7] Patten J, Fesperman R, Kumar S, McSpadden S, Qu J, Lance M, et al. Appl Phys Lett 2003;83:4740.
[8] Jamieson JC. Science 1963;139:338.
[9] Chang KJ, Cohen ML. Phys Rev B 1985;31:7819.
[10] Hu JZ, Merkle LD, Menoni CS, Spain IL. Phys Rev B 1986;34:4679.
[11] Olijnyk H. Phys Rev Lett 1992;68:2232.
[12] Crain J, Ackland GJ, Maclean JR, Piltz RO, Hatton PD, Pawley GS. Phys Rev B 1994;50:13043.
[13] Piltz RO, Maclean JR, Clark SJ, Ackland GJ, Hatton PD, Crain J. Phys Rev B 1995;52:4072.
[14] Gridneva V, Milman YV, Trefilov VI. Phys Stat Sol (a) 1972;9:177.
[15] Gerk AP, Tabor D. Nature 1978;271:732.

[16] Clarke DR, Kroll MC, Kirchner PD, Cook RF, Hockey BJ. Phys Rev Lett 1988;60:2156.
[17] Pharr GM, Oliver WC, Clarke DR. Scripta Mater 1989;23: 1949.
[18] Pharr GM, Oliver WC, Harding DS. J Mater Res 1991;6:1129.
[19] Pharr GM, Oliver WC, Cook RF, Kirchner PD, Kroll MC, Dinger TR, et al. J Mater Res 1992;7:961.
[20] Page TF, Oliver WC, McHargue CJ. J Mater Res 1992;7:450.
[21] Callahan DL, Morris JC. J Mater Res 1992;7:1614.
[22] Wepplmann ER, Field JS, Swain MV. J Mater Res 1993;8:450.
[23] Wepplmann ER, Field JS, Swain MV. J Mater Sci 1995;30:2455.
[24] Kailer A, Gogotsi YG, Nickel KG. J Appl Phys 1997;81:3057.
[25] Wu YQ, Xu YB. J Mater Res 1999;14:2262.
[26] Wu YQ, Yang XY, Xu YB. Acta Mater 1999;47:2431.
[27] Mann AB, van Heerden D, Pethica JB, Weihs TP. J Mater Res 2000;15:1754.
[28] Mann AB, van Heerden D, Pethica JB, Bowest P, Weihs TP. Philos Mag A 2002;82:1921.
[29] Ge D, Domnich V, Gogotsi Y. J Appl Phys 2003;93:2418.
[30] Ge D, Domnich V, Gogotsi Y. J Appl Phys 2004;95:2725.
[31] Zarudi I, Zhang LC. Tribol Int 1999;32:701.
[32] Bradby JE, Williams JS, Wong-Leung J, Swain MV, Munroe P. Appl Phys Lett 2000;77:3749.
[33] Bradby JE, Williams JS, Wong-Leung J, Swain MV, Munroe P. J Mater Res 2001;16:1500.
[34] Lloyd SJ, Molina-Aldareguia JM, Clegg WJ. J Mater Res 2001;16:3347.
[35] Saka H, Shimatani A, Suprijadi Suganuma M. Philos Mag A 2002;82:1971.
[36] Zarudi I, Zhang LC, Swain MV. J Mater Res 2003;18:758.
[37] Zarudi I, Zou J, Zhang LC. Appl Phys Lett 2003;82:874.
[38] Smith GS, Tadmor EB, Kaxiras E. Phys Rev Lett 2000;84:1260.
[39] Smith GS, Tadmor EB, Bernstein N, Kaxiras E. Acta Mater 2001;49:4089.
[40] Bradby JE, Williams JS, Swain MV. Phys Rev B 2003;67:085205.
[41] Kailer A, Nickel KG, Gogotsi YG. J Raman Spect 1999;30:939.
[42] Domnich V, Gogotsi Y, Dub S. Appl Phys Lett 2000;76:2214.
[43] Gogotsi Y, Domnich V, Dub S. J Mater Res 2000;15:871.
[44] Juliano T, Gogotsi Y, Domnich V. J Mater Res 2003;18:1192.
[45] Domnich V, Gogotsi Y. Rev Adv Mater Sci 2002;3:1.
[46] Oliver WC, Pharr GM. J Mater Res 1992;7:1564.
[47] Zi J, Büscher H, Falter C, Ludwig W, Zhang K, Xie X. Appl Phys Lett 1996;69:200.
[48] Sneddon IN. Int J Eng Sci 1965;3:47.
[49] Johnson KL. Contact mechanics. Cambridge: Cambridge University Press; 1985. p. 107.
[50] Jang JI, Wen S, Lance MJ, Anderson IM, Pharr GM. Mater Res Soc Symp Proc 2004;795:313.
[51] Johnson KL. J Mech Phys Solids 1970;18:115.
[52] Galanov BA, Domnich V, Gogotsi Y. Exp Mech 2003;43:304.